



Deposited via The University of Sheffield.

White Rose Research Online URL for this paper:

<https://eprints.whiterose.ac.uk/id/eprint/227496/>

Version: Accepted Version

Article:

Gapp, S., Schnalzger, G., Maierhofer, J. et al. (2025) Wear mechanisms and transitions in advanced railway materials - a twin disc benchmark of Mn13, CrB1400 and R400HT. *Wear*, 564-565. 205713. ISSN: 0043-1648

<https://doi.org/10.1016/j.wear.2024.205713>

© 2024 The Authors. Except as otherwise noted, this author-accepted version of a journal article published in *Wear* is made available via the University of Sheffield Research Publications and Copyright Policy under the terms of the Creative Commons Attribution 4.0 International License (CC-BY 4.0), which permits unrestricted use, distribution and reproduction in any medium, provided the original work is properly cited. To view a copy of this licence, visit <http://creativecommons.org/licenses/by/4.0/>

Reuse

This article is distributed under the terms of the Creative Commons Attribution (CC BY) licence. This licence allows you to distribute, remix, tweak, and build upon the work, even commercially, as long as you credit the authors for the original work. More information and the full terms of the licence here: <https://creativecommons.org/licenses/>

Takedown

If you consider content in White Rose Research Online to be in breach of UK law, please notify us by emailing eprints@whiterose.ac.uk including the URL of the record and the reason for the withdrawal request.

Highlights

Wear mechanisms and transitions in advanced railway materials - a twin disc benchmark of Mn13, CrB1400 and R400HT

Sebastian Gapp, Georg Schnalzger, Jürgen Maierhofer, Werner Daves, Kazim Yildirimli, Roger Lewis

- Wheel-rail contact
- Wear
- Twin disc tests
- Advanced crossing materials
- Switches & Crossings

Wear mechanisms and transitions in advanced railway materials - a twin disc benchmark of Mn13, CrB1400 and R400HT

Sebastian Gapp^{a,*}, Georg Schnalzger^a, Jürgen Maierhofer^a, Werner Daves^a, Kazim Yildirimli^b and Roger Lewis^b

^aMaterial Center Leoben Forschung GmbH, Leoben, A-8700, Austria

^bDepartment of Mechanical Engineering, University of Sheffield, Sheffield, UK-S10 2TN, UK

ARTICLE INFO

Keywords:

Wheel-rail contact

Wear

Twin disc tests

Crossing materials

Switches & Crossings

ABSTRACT

In order to ascertain the wear behavior of three advanced crossing materials, twin disc tests are conducted. In particular, the austenitic Hadfield manganese steel Mn13, the ultrafine-pearlitic R400HT and the chromium bainitic CrB1400 steel are benchmarked. The investigated crossing materials are combined with the standard wheel material ER7. Due to the relatively low initial hardness of the as-cast Mn13 the crossings are typically pre-hardened by the explosive depth hardening technique. Due to the size of the discs, explosive depth hardening the Mn13 disc is not a viable option. R400HT is identified as exhibiting the greatest resistance to wear, although CrB1400 demonstrated comparable results. Mn13 showed the highest wear rates. Three primary reasons for the elevated wear rates of Mn13 have been identified. These include a significantly lower initial hardness, a distinct hardening mechanism in conjunction with a high work hardening potential and a different wear mechanism that demonstrated a high dependency on the applied contact pressure.

1. Introduction

The possibility to maneuver between different rail tracks is enabled by switches and crossings (S&C). Therefore, these components are indispensable for the flexibility of a railway network. The frequently reoccurring rolling sliding contact between wheel and rail drives three main damage mechanisms, namely wear, plastic deformation and rolling contact fatigue (RCF) [1]. Furthermore, the contact conditions and therefore the damage is influenced by geometrical changes due to plastic deformations of the contact partners [2]. Due to the discontinuities in track that occur with the installation of S&C, exceptional high dynamic loads between wheel and rail are the consequences [3]. Higher damage rates with respect to wear and RCF emerge from the dynamic load peaks. To ensure the safety of turnouts, tight inspection and maintenance intervals are required, which lead to an increase of operational costs [4].


The dynamic impact caused by the transfer of the wheel from the wing rail to the crossing nose, results in high stresses, varying rolling radii (slip) and dynamic normal and lateral contact forces. These conditions demand highly engineered materials to provide more resistance to the damage modes expected. Premium rail steels are applied to withstand the loading, enlarge the maintenance intervals and reduce life cycle costs (LCC) of these components.

Within this work three advanced crossing materials are tested using twin disc tests. In particular, the austenitic Hadfield manganese steel Mn13, the ultrafine-pearlitic R400HT and the chromium bainitic CrB1400 steel are benchmarked. The main mechanical properties of the tested materials are

provided in Table 1 [5–8]. The mechanical properties of Mn13 significantly differs from the other two rail steel grades: CrB1400 and R400HT exhibit a rather high initial hardness and tensile strength compared to Mn13. However, the elongation, an indicator for the work hardening capability in service, is significantly higher for Mn13. The difference is mainly caused by different hardening mechanisms: The pearlitic and bainitic microstructure primarily strain hardens when subjected to plastic deformation due to the dislocation movement. Mn13 primarily work hardens by the so-called twinning-induced plasticity (TWIP), a cold working mechanism, which leads to a significantly higher work hardening capability [9, 10]. Due to this characteristics Mn13 is mainly used in the frog of turnouts. The high compressive dynamic loads during the wheel passage cause a steady increase of the material hardness as well as a geometrical adaption of the contact geometries leading to a lower local contact loading, e.g. [5, 9]. Due to the comparably low initial hardness of as-cast Mn13 the frogs are mostly pre-hardened by the technique of explosive depth hardening (EDH) leading to hardness values of up to 400 HBW, which is comparable to the high strength materials CrB1400 and R400HT [11]. However, to the best-knowledge of the authors currently no EDH technique is available for small-scale samples required for laboratory twin disc tests. Therefore, the Mn13 is considered in its as-cast condition.

Twin disc testing is a widely spread approach to benchmark railway materials under a broad variety of realistic rolling-sliding loading conditions as they occur in track [12–15]. The twin disc setup is appropriate to reproduce the main damage mechanisms observed in wheel-rail contact on a laboratory scale. Therefore, twin disc tests are a cost-efficient method to study the wear mechanisms and quantify wear rates for different materials [16, 17]. In addition, twin disc tests are frequently applied to study the initiation of RCF

*Corresponding author

 sebastian.gapp@mcl.at (S. Gapp)

 www.mcl.at (S. Gapp)

ORCID(s): 0009-0001-8009-0047 (S. Gapp)

Table 1
Mechanical properties of the investigated rail and wheel steels [5–8]

	Hardness [HBW]	Tensile strength [MPa]	Elongation [%]
R400HT	440-490	≥ 1350	≥ 8
Mn13 (as-cast)	220	≥ 725	≥ 30
CrB1400	420-480	≥ 1400	≥ 11
ER7	250-270	≥ 900	≥ 14

cracks and the effect of friction modifiers [13, 14, 18, 19]. A drawback of the downsizing is the transfer of results from laboratory to the track due to the non-linear nature of contact mechanics. However, researches have optimized sample geometries [16] and introduced several approaches such as the T-Gamma value to characterize wheel-rail contact conditions, identify different wear regimes and transfer results between different scales [17]. Nevertheless, the surface roughness cannot be scaled properly due to the limited disc size leading to differences in the subsurface stress distribution, which has an impact on the damage initiation that must be considered when assessing test results [20].

Standard railway materials have been intensively investigated using twin-discs [17, 21–23]. However, twin disc results especially regarding the wear mechanism for the advanced materials considered in this study are limited. Researchers have already investigated the wear behavior of R400HT in twin disc tests, e.g. in [13, 24]. The investigated wear mechanism is comparable to the standard pearlitic rail steel grades such as the grade 900A [25] as well as the standard wheel materials (e.g., ER7) [26]. Messaadi et. al. [27] conducted a twin disc test on CrB1400, focusing on the influence of friction modifiers. Data regarding the wear behavior, especially with respect to the dominating wear mechanism, are currently missing in literature. For Mn13 wear data is available from ball on disc [28] as well as dry reciprocal sliding tests [29]. The wear mechanism is expected to differ from the other two materials investigated in the twin-disc test due to the formation of twins within the grains, as reported for comparable materials subjected to similar loading conditions. In general, higher wear rates are expected due to the low initial hardness and work hardening mechanism based on the results published in literature. [30–32]

Previous works [17, 25, 33, 34] identified three typical wear regimes for wheel and rail steels under rolling-sliding contact, namely *mild*, *severe* and *catastrophic* wear. The dominating wear regime is mostly depending on contact pressure, slip, materials in contact and temperature in the contact zone [17]. The transition of wear is a consequence of differing contact conditions. In the contact between the wheel tread and the rail head, it is probable that both mild and severe wear will occur. When the wheel flange and rail gauge corner are in contact, a phenomenon known as full slip may occur, which can result in severe to catastrophic

wear. Moreover, thermal material softening, which results in catastrophic wear, can be initiated by high temperatures that result from high slip conditions in the wheel/rail contact [34]. Furthermore, wear is related to different mechanisms occurring in the wheel/rail contact. These include the following types of wear: abrasive, adhesive, delamination, tribo-chemical, fretting, surface fatigue and impact [35].

2. Methods

Wear tests were carried out on the Sheffield University Rolling Sliding (SUROS) twin disc test rig. A line contact is used between twin disc test specimens on this machine to simulate the contact stress and rolling-sliding slip conditions seen at the wheel/rail interface. This section describes the test methodology and the machine setup of the used SUROS. A brief description of the SUROS machine can be found in [36]. In addition, details about the tested specimens and the test approach itself are presented.

2.1. Test apparatus

A twin disc test consists of a driving (faster) and a driven (slower) disc. Both discs are driven by an AC motor to achieve a difference in speed and consequently slip between the discs [36, 37].

As in several previous works [14, 21, 22, 38–40] that focused on damage mechanisms in the wheel-rail contact, the SUROS test machine of the University of Sheffield is used for this test series. The possible disc speed ranges from 0 to 1600 rpm and a maximum load of 29 kN can be applied. Figure 1 shows the mechanical setup of a twin disc apparatus.

2.2. Twin disc specimens

The discs are manufactured from wheel and rail components as close as possible to the wheel rail contact positions. Therefore, the wheel discs are cut out near the running surface at the wheel rim. In a similar process the R400HT and CrB1400 rail discs are sectioned out of a 60E1 rail head. The Mn13 discs are cut out of a non-EDH cast block, which is manufactured in a special process to achieve similar material properties as in as-cast crossing noses. However, in comparison to the real crossing nose, the EDH process is not applicable for the cast block.

The discs have an outer diameter of 47 mm and a cylindrical running width of 10 mm. Figure 2 illustrates the cut out regions of the specimens and the according dimensions of the discs. The average roughness R_a on the contact surfaces of the discs is below $0.5 \mu\text{m}$. Due to the relatively small diameter of the discs, it is not feasible to harden the Mn13 discs using an EDH process as it would cause damage. Therefore, it is noted that the comparison to the behavior of the real crossing nose may be limited.

2.3. Test conditions

The materials are tested at a constant reference speed of 400 rpm resulting in a surface speed of 1 m/s. Two normal

Table 2
Testing parameters

	Wheel material	Rail material	Contact pressure [MPa]	Slip [%]	Disc speed [rpm]
1	ER7	R400HT	1 400	0.5	400
2	ER7	Mn13	1 400	0.5	400
3	ER7	CrB1400	1 400	0.5	400
4	ER7	R400HT	1 800	0.5	400
5	ER7	Mn13	1 800	0.5	400
6	ER7	CrB1400	1 800	0.5	400

Adam Equipment Co. Ltd. Model AAA30L, is then used to calculate wear rates. During the tests, after each block of cycles, the tests were stopped and the mass and diameter of discs were recorded again. Surface roughness values were measured, and tests were continued. The post-test analyses include the evaluation of grain deformation and material hardness. A scanning electron microscope (SEM) of type TM3030 Hitachi Tabletop is used to analyze the wear debris. After 50 000 cycles grain deformations are visualized with a optical microscope of type Nikon Eclipse LV 150. The post-test hardness measurements are conducted with micro- and nano-indentation tests. The hardness measurements are performed with DuraScan micro-hardness and Bruker nano-hardness of type Hysitron test machines, respectively. A Vickers indenter is applied for these tests. After all blocks of cycles in each test were finished, the mass, diameter of the discs, and roughness measurements were recorded. Discs were then sectioned for further analysis. The samples were mounted, ground and polished. Micro- and nano- hardness measurements were carried out and after that, the samples were etched with a 2 % Nital solution for microstructure analysis using a scanning electron microscope.

3. Results

This section presents the test results. In particular the following parameters are evaluated: wear rates, analysis of wear debris, plastic deformations and microstructural changes, friction values and material hardness.

3.1. Wear rates

The wear rates of the tested crossing materials are evaluated over the rolling cycles. Figure 3 illustrates the wear rate evolution for R400HT, Mn13 and CrB1400. Figure 3a and b show the rail wear rates and Figure 3c and d the wheel wear rates, respectively. The diagrams on the left hand side account for an applied contact pressure of 1 400 MPa and the right hand sided ones for 1 800 MPa.

At a contact pressure of 1 400 MPa, R400HT and CrB1400 show similar rail wear rate curves. A clear plateau is not reached for these two materials although the wear rate increase is reduced after 10 000 cycles. The Mn13 specimen shows a significantly higher wear rate.

In Figure 3b R400HT and CrB1400 show again a quantitatively similar behavior of rail wear rates. The wear rate at the end of the 1 400 and 1 800 MPa tests is about 4 $\mu\text{g}/\text{cycle}$. Therefore, the wear behavior of R400HT and CrB1400 seems to be almost independent of the applied contact pressure. In both cases R400HT has the least total wear. Mn13 shows a completely different behavior compared to 1 400 MPa. The wear rates of Mn13 increase almost linearly over the cycles and show no sign of reaching a constant wear rate. A maximum of nearly 30 $\mu\text{g}/\text{cycle}$ is reached, which is significantly higher than that of the other crossing materials. Comparing Figure 3a and b, Mn13 shows a high sensitivity to the applied contact pressure.

For all materials in Figure 3c the wheel wear rates increase linearly for the first 30 000 cycles. A plateau is reached as the test cycles progress, resulting in a wheel wear rate of approximately 10 $\mu\text{g}/\text{cycle}$ for R400HT and CrB1400. Mn13 shows a qualitatively similar behavior although the increase in wear rate is higher between 10 000 and 30 000 cycles. Mn13 reaches a constant wheel wear rate of about 14 $\mu\text{g}/\text{cycle}$ after 30 000 cycles.

Compared to Figure 3b, Figure 3d shows a similar behavior of Mn13 related wear rates, where no constant wear behavior is noticeable. A maximum of about 26 $\mu\text{g}/\text{cycle}$ is reached and therefore significantly higher than the maximum wheel wear rates of R400HT and CrB1400, respectively. Consequently, the wheel wear rate of Mn13 also shows a clear dependence on the applied contact pressure. In this setup CrB1400 does not reach a clear plateau, on the contrary the wheel wear rate keeps increasing over cycle numbers. The wheel wear rate of R400HT tends to settle at 6 $\mu\text{g}/\text{cycle}$.

3.2. Wear debris

A focus of this experimental series is the analysis of the wear debris. Figure 4 and Figure 5 show SEM images of the wear debris produced at various stages of the tests. Figure 4 refers to a normal load of 1 400 MPa and Figure 5 to 1 800 MPa, respectively. The images show both the rail and wheel debris. Therefore, it is not clear if the rail or wheel material formed certain flakes.

After 10 000 cycles at 1 400 MPa it seems that ER7-R400HT formed many but small flakes. The flakes of ER7-CrB1400 and ER7-Mn13 are bigger but fewer. This is in good agreement with the wear rate curves, see Figure 3a and c, which do not show a clear difference at this stage. Between 10 000 and 30 000 cycles ER7-R400HT and ER7-CrB1400 formed more flakes than ER7-Mn13. Since the total wear between 10 000 and 30 000 cycles is higher for the Mn13 tests, it follows that these flakes need to be significantly bigger, which is proven by the SEM images. The presence of these large particles, measuring several hundred micrometers, in the contact area may result in the development of third body abrasive wear, which is characterized by elevated wear rates compared to two-body abrasive wear. Moreover, the particles may become embedded on the running surface of a disc. This results in an increase of the surface roughness, which in turn leads to a higher wear rate. Comparing the

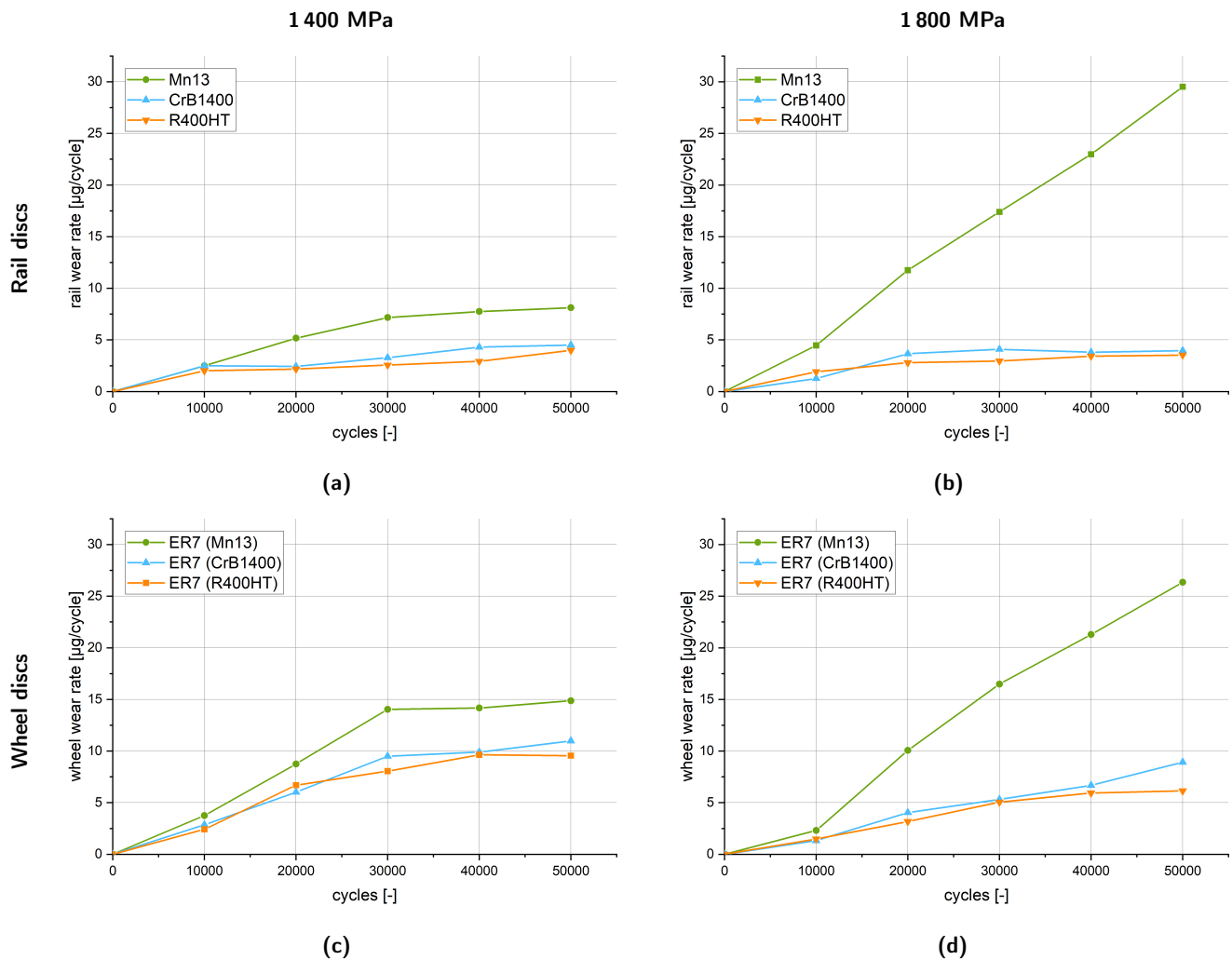


Figure 3: Wear rates of rail ((a) and (b)) wheel discs ((c) and (d)) at 1400 MPa ((a) and (c)) and 1800 MPa ((b) and (d)), respectively. The materials are divided by the color code.

images after 10 000 and 50 000 cycles, the particles size of all three materials increased with the cycle number.

Unfortunately, the image for R400HT after 10 000 cycles at 1 800 MPa is not available in Figure 5. In the first 10 000 cycles, ER7-Mn13 formed more but smaller flakes compared to ER7-CrB1400. This is in good agreement with the wear rate curves, see Figure 3b and d, which show a higher total wear for ER7-Mn13. After 30 000 cycles ER7-R400HT formed the least flakes. The quantity and size of ER7-Mn13 flakes is the highest, as evidenced by the significantly higher wear rates. The images after 50 000 cycles correspond to the trend after 30 000 cycles. For ER7-Mn13, the flakes appear to be smaller compared to 1 400 MPa. Based on the three body abrasive wear theory, the flakes probably got crushed by the higher contact pressure.

3.3. Deformation analysis

To gain a comprehensive understanding of the material behavior under the twin disc test conditions, the authors conducted a subsurface analysis by capturing microscope

images of the internal structure of the tested crossing materials. These subsurface images unveil information regarding potential subsurface damage and wear mechanisms. Therefore, the discs are cut and etched using a 2 % Nital solution. Figure 6 illustrates the methodology employed for the extraction of metallographic cross-section samples from the discs. In Figure 7 the optical microscope images of cut and etched rail discs after 50 000 cycles are shown.

For R400HT in Figure 7a and b the images show minor plastic deformations with a depth of approximately $100 \mu\text{m}$. Furthermore, short and shallow cracks are visible. The substructure and the deformed layer exhibit comparable characteristics at both contact pressures. These images serve to reinforce the similarity observed in the rail wear rates. Figure 7c illustrates that Mn13 at 1 400 MPa exhibits a deformed grain structure, yet no cracks. In comparison to R400HT and CrB1400 the grains are larger, which is a consequence of the casting process. The distinctive microstructural characteristics of Mn13 are highlighted in Figure 7c and d. Formed twins are clearly visible. Moreover, inclusions are marked and a possible grain boundary crack could be

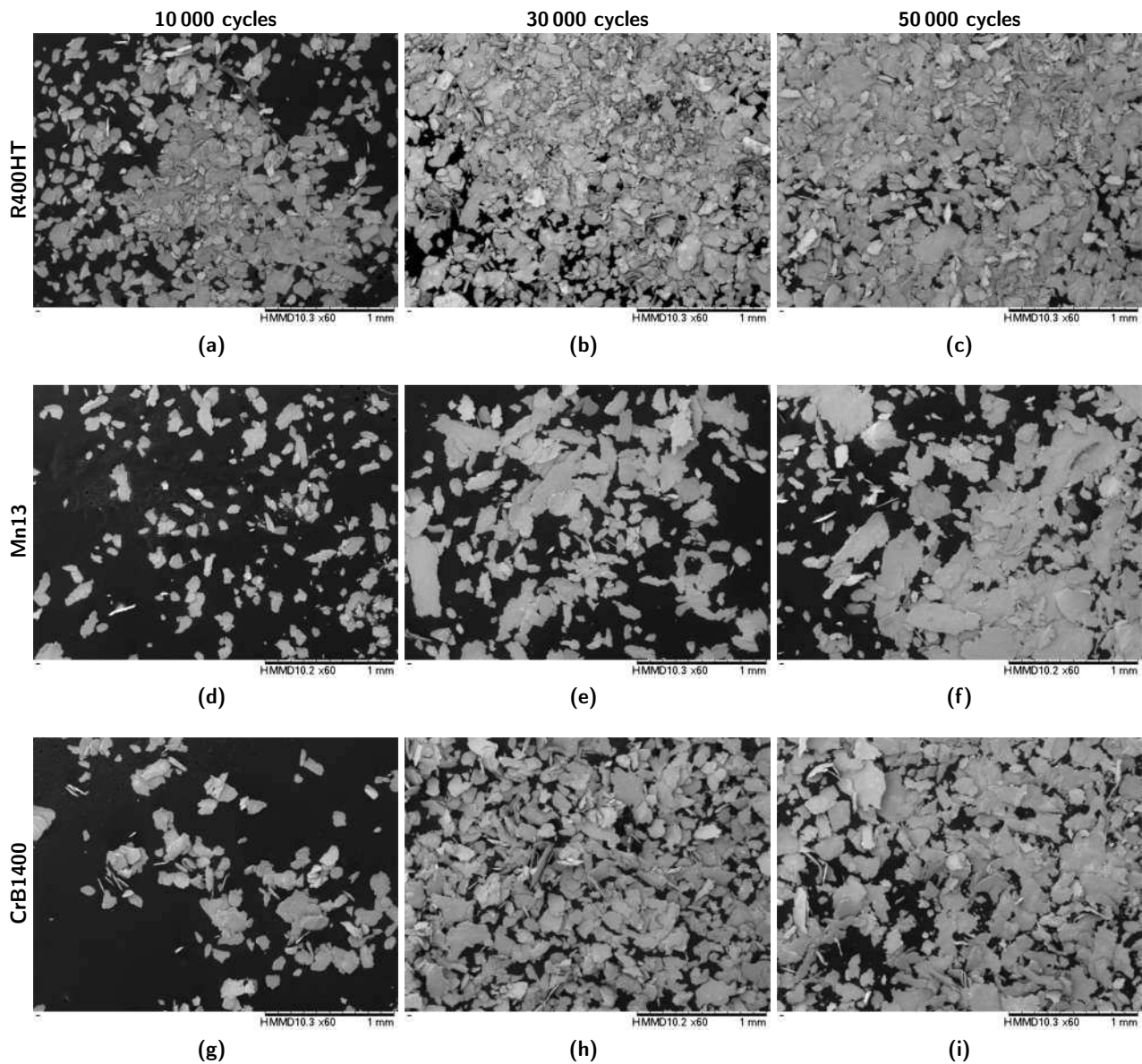


Figure 4: SEM images of wheel and rail wear debris for 1400 MPa of contact pressure.

determined in Figure 7d. Lindross et. al. [31] observed comparable metallographic characteristics in high manganese steel samples. Nevertheless, the testing conditions are quite distinct. **Is that sentence correct from a metallographic perspective?**

As illustrated in Figure 7e and f, according to CrB1400, there are small deformation layers and some short, shallow cracks are visible. The deformation depth is approximately 70-80 μm . As with the R400HT, the substructure and plastic deformation are comparable, which aligns with the results of the rail wear rate diagrams in Figure 3.

3.4. Friction values

The coefficients of friction (COF) are determined by the friction force every 10000 cycles. The friction force is measured via torque measurements on one of the shafts and data is collected throughout the test. Further details

can be found in [36]. The COFs represented in Table 3 are determined by averaging between 30000 and 50000 cycles to account for a run-in state. The different contact conditions that occur between wheel and rail/crossing can affect the COF. All materials show lower values for a higher contact pressure, which is in good agreement with previous works, e.g. [41]. The correlation of COF for R400HT and CrB1400 underline the similarity in the wear rates of these two materials. The significantly higher wear rates observed for Mn13 cannot be attributed to the evaluated COFs, which again indicates the presence of a distinct wear mechanism.

3.5. Hardness

The HV1 micro hardness profiles of Mn13, R400HT and CrB1400 were determined at various material depths. Figure 8 shows the hardness distribution for the tested materials after 50000 cycles.

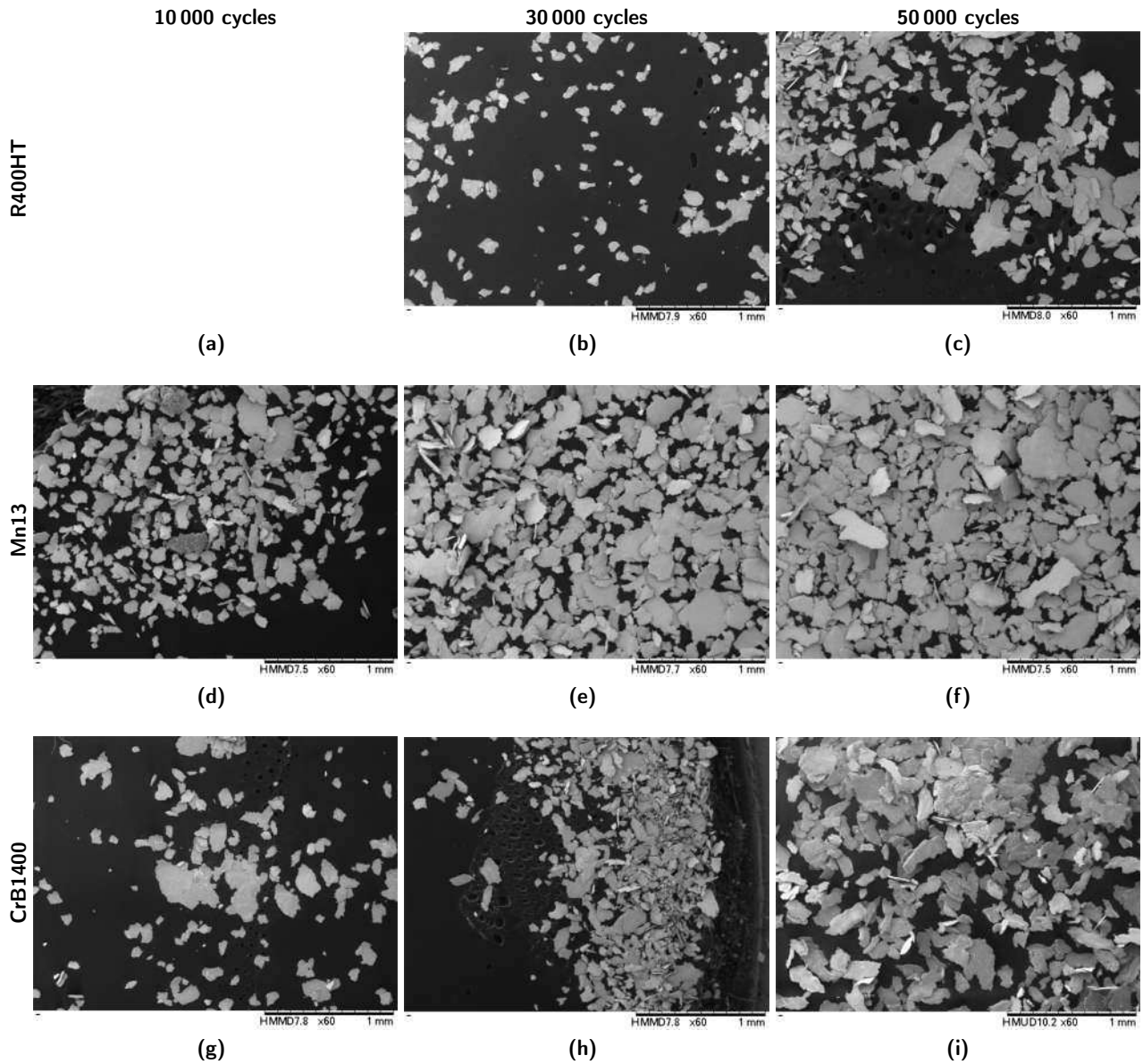


Figure 5: SEM images of wheel and rail wear debris for 1800 MPa of contact pressure.

Table 3

Coefficients of friction: Average values between 30 000 and 50 000 cycles.

	1 400 MPa	1 800 MPa
R400HT	0.30	0.25
Mn13	0.32	0.23
CrB1400	0.28	0.23

In both cases, the hardness distribution of R400HT and CrB1400 is nearly constant. Given that these materials have undergone heat treatment, which has resulted in a high bulk hardness and consequently a low work hardening potential, this result is reasonable. Except for CrB1400 at 1 800 MPa all materials have the highest hardness on the surface. This increase follows from the cyclic loading of the discs. Mn13

shows a clear hardness gradient. In a depth of 3 mm the bulk hardness of Mn13 amounts to about 235 HV. In a depth of about 1.5 mm the hardness starts to stabilize. Consequently, the first 1.5 mm are affected by the cyclic rolling contact load. In this region the twinning process leads to the increased hardness. The maximum measured micro hardness value is about 575 HV directly below the surface of the Mn13 disc in Figure 8b.

Since it is difficult to position the micro-indenter near the surface, nano-indentation hardness measurements are performed to verify the surface hardness. Therefore, higher resolution of the hardness distribution near the surface is available. An example how the nano-indentation measurements are performed is given in Figure 9. Within the red marked $50 \mu\text{m} \times 50 \mu\text{m}$ square, a 10×10 array of indentations is visible. The indentations are placed as close as possible to the transition zone of bakelite and specimen. The specimen

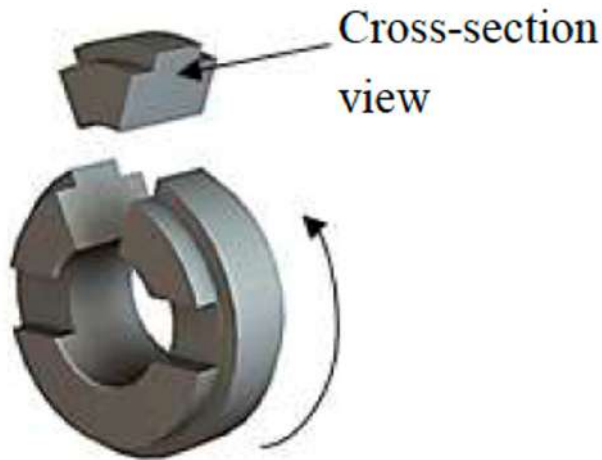


Figure 6: Exemplary representation of the analyzed disc section. **Will be redrawn!**

Table 4
Results of the nano-hardness measurements.

Material	Contact pressure [MPa]	Indentation force [μN]	Surface hardness [HV]
R400HT	1 400	3 000	1 019
R400HT	1 800	3 000	1 049
Mn13	1 400	3 000	927
Mn13	1 800	3 000	958
CrB1400	1 400	5 000	968
CrB1400	1 800	5 000	948

is mounted in the bakelite. The evaluated nano-hardness values correspond to the data point that is closest to the surface.

In Table 4 the results are summarized. The highest surface hardness is reached by R400HT. Since R400HT shows slightly less wear this correlates with the hardness measurements. However, all hardness values are in a similar range. Except for CrB1400, the surface hardness of all materials increased with the contact pressure, which correlates micro-hardness measurements represented in Figure 8.

4. Discussion

The results indicate that R400HT and CrB1400 exhibit lower wheel and rail wear rates compared to Mn13. This suggests that R400HT and CrB1400 demonstrate superior wear resistance under the specified test conditions. Moreover, the wear rate of Mn13 increases significantly with the contact pressure. Previous studies emphasized the potential and equivalence of Mn13 crossings to other materials [5, 42, 43]. In addition to the disparate load conditions between a crossing application and a twin-disc test, several potential explanations for these elevated Mn13 wear rates are presented.

4.1. Differences in the wear behavior

As outlined by Bolton and Clayton [33], the presence of large and thin flakes is indicative of their so-called type I rolling-sliding wear, also known as mild wear. This type of flake is formed by a ratchetting process, whereby plastic deformation leads to the formation of shallow cracks and subsequent material removal. These kind of cracks are evident in the R400HT and CrB1400 samples, as illustrated in Figure 7. Moreover, Figure 4 and Figure 5 demonstrate the presence of large and thin flakes in all samples. However, since Mn13 does not indicate shallow cracks or a comparable deformation layer, this indicates that a different wear mechanism is at play. This is evidenced by the observation that Mn13 shows almost no deformation, especially at 1 800 MPa (Figure 7d), which suggests that ratchetting did not occur and consequently flakes might not be formed. Given inability to distinguish debris between rail and wheel material, it is possible that the ER7-Mn13 flakes shown in Figure 4 and Figure 5 are, in fact, mostly ER7 flakes. Based on these observations, the austenitic Mn13 appears to have a different damage mechanism in comparison to pearlitic R400HT and bainitic CrB1400. It is likely that the Mn13 experiences wear via a more typical mechanism, such as adhesive or abrasive wear. These mechanisms are significantly affected by the contact force, which explains the higher wear observed at 1 800 MPa compared to 1 400 MPa, see Figure 3.

The $T\gamma/A$ numbers, which give an indication of the energy within the contact, are calculated for all test conditions and at each time the experiments are stopped. T refers to the tangential force in the contact, γ is the dimensionless slip and A marks the contact area. The values show little variation and are between 1.0 and 1.9 N/mm^2 for all performed twin disc tests. It can be reasonably assumed that similar $T\gamma/A$ values would lead to comparable wear results for the same material combination, despite differences in the conditions (load and slip) employed to generate these results [37]. This is evident in the case of CrB1400 and R400HT, where the wear rates exhibit minimal variation between 1 400 MPa and 1 800 MPa. Conversely, for Mn13, this is not the case, which again highlights a distinction in the wear mechanism.

4.2. Influence of material hardness

According to the most frequently used Archard wear equation, the wear depth Δz follows from Equation 1:

$$\Delta z = k \frac{|s|p}{H} \quad (1)$$

where k is the wear coefficient, s is the sliding distance, p is the contact pressure and H is the material hardness. According to this wear law, the amount of wear is inversely proportional to the material hardness. In summary, harder materials tend to result in less wear. Considering that Mn13 has an initial hardness that is approximately half that of R400HT or CrB1400, the higher rail wear rates at 1 400 MPa in Figure 3a appear reasonable. The rail wear rate of Mn13 after 50 000 cycles is twice that of the other materials, in accordance with Archard's wear law. It is important to

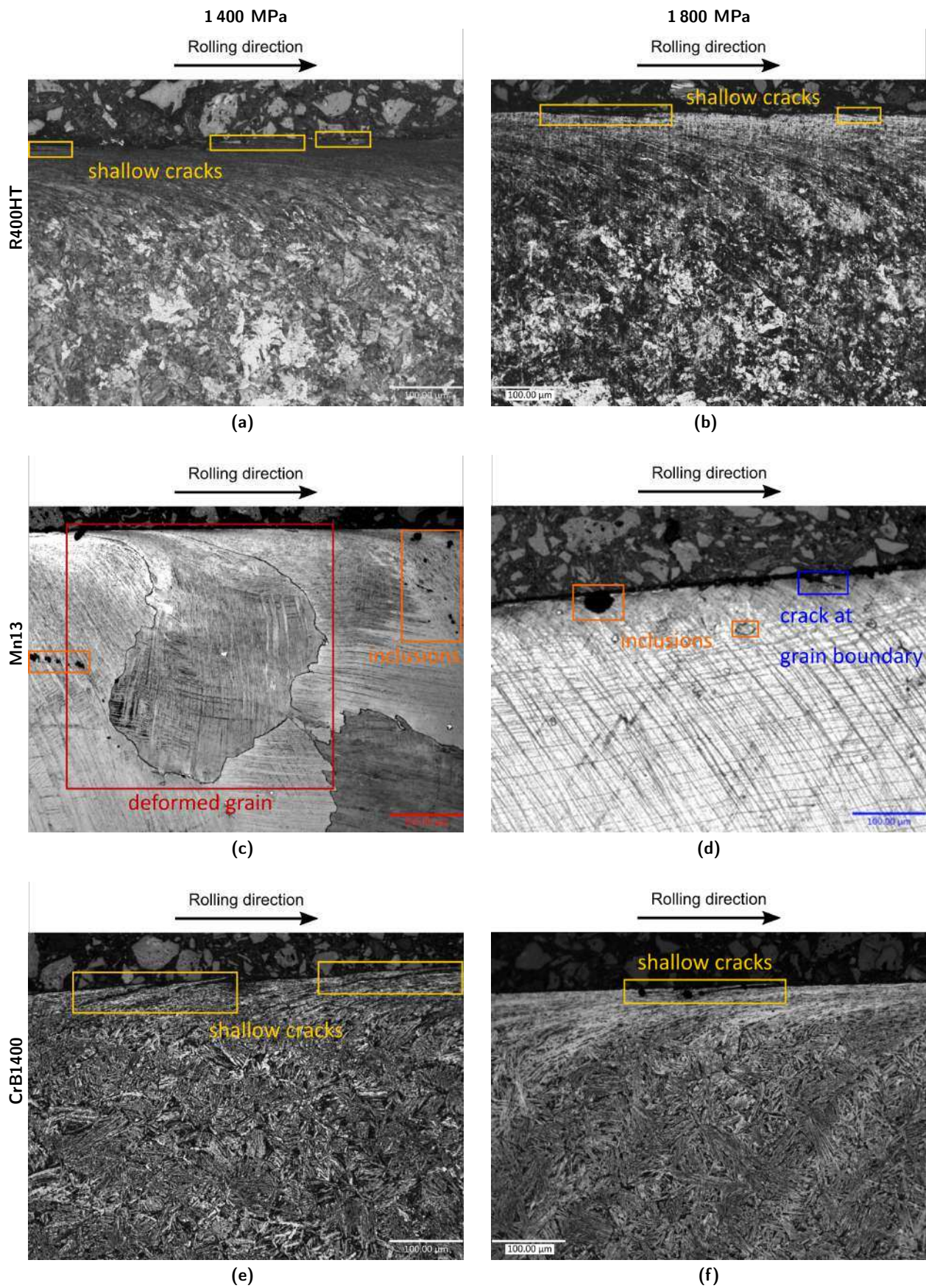


Figure 7: Images of cross-sectionally cut and etched rail discs obtained using a light microscope. The metallographic characteristics of the samples are marked.

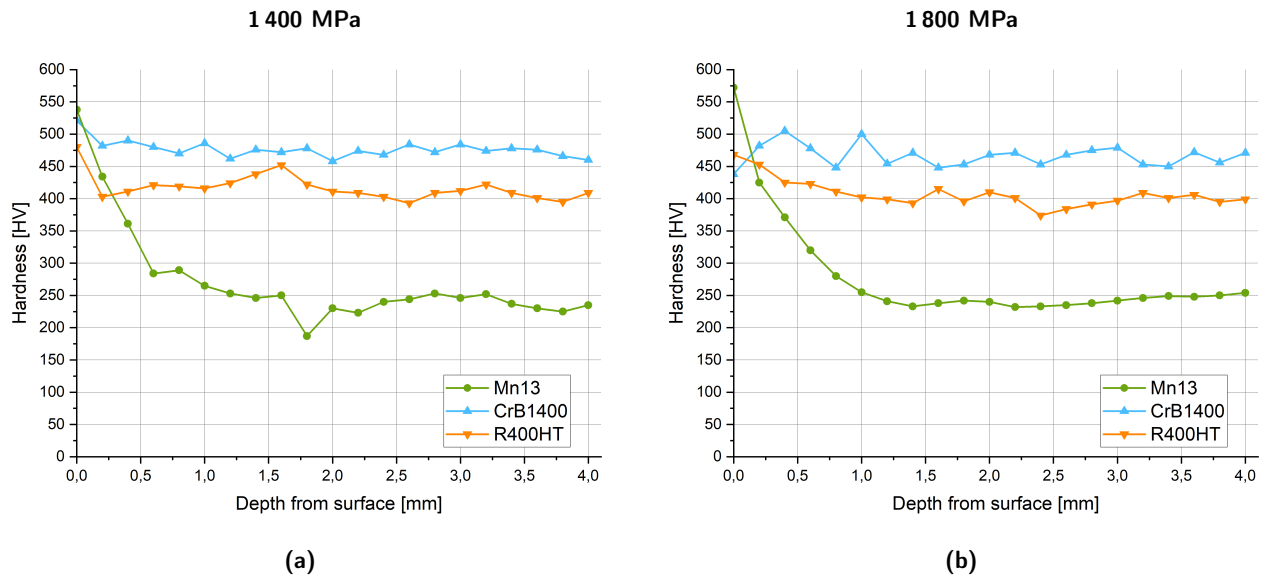


Figure 8: Hardness measurements analyzed over the depth after 50 000 cycles. Subfigure (a) accounts for a contact pressure of 1 400 and (b) for 1 800 MPa, respectively.

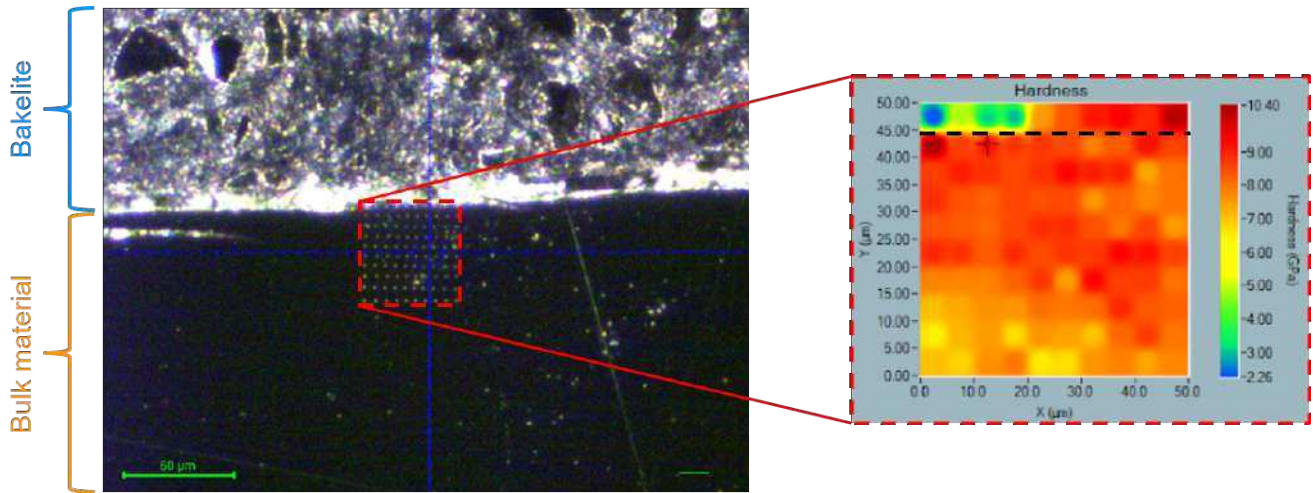


Figure 9: Example for the performed nano-indentation hardness measurements for CrB1400 at a contact pressure of 1 800 MPa. The brighter region at the top of the left image shows the bakelite, where the specimen is mounted in. The red marked square has a size of $50 \mu\text{m} \times 50 \mu\text{m}$. Within this square a 10×10 array of nano-indentations is performed. The right diagram shows the hardness evaluation. The black dotted line represents the transition to the bakelite.

note that Mn13 crossings are typically pre-hardened with EDH. Manganese crossings that undergo EDH hardening can achieve hardness values within the range of the R400HT and CrB1400, as evidenced by research [11]. It is therefore anticipated that the rail wear rate at 1 400 MPa will decrease and fall within the range of R400HT and CrB1400. Consequently, EDH is advised for Mn13 crossings in order to achieve comparable hardness. Nevertheless, to date, there is no evidence of EDH processing of twin disc specimens. For an applied contact pressure of 1 800 MPa, it appears that the difference in wear mechanisms has a greater influence on the wear behavior than the material hardness. However, it is assumed that a higher initial hardness would also result in a decreased wear rate at higher contact pressures.

As stated by Lewis et. al. [23], the wheel wear rate increases with the rail hardness only when the rail is softer. Since the initial hardness of Mn13 is lower than that of ER7, the increasing hardness due to the TWIP work hardening process of Mn13 could result in an elevated wheel wear rate. However, the authors believe that the difference in wear mechanism is the main reason for the significantly higher wear rates.

Although the surface hardness of all rail discs are comparable after 50 000 cycles, it is unclear, at which cycle number this hardness is reached, especially for Mn13. Figure 3a and c show that the rail and wheel wear rates of Mn13 stabilize after 30 000 cycles. This may indicate that the twinning process reached saturation at a surface hardness

level that is comparable to R400HT and CrB1400. However, for Figure 3b and d the wear rates of Mn13 do not stabilize. Therefore, the full work hardening potential at 1 800 MPa is not yet reached, as stated in [23]. Consequently, as mentioned in the introduction, the different hardening mechanism may be an additional factor contributing to the observed differences in wear behavior.

The measurements of surface hardness obtained through micro- and nano-indentation techniques yield disparate results. As described by Qian et. al. [44], this phenomena is a so-called scaling effect. The reason is that metals show strong indentation size effects. Determining the significance of Mn13 surface hardness is challenging due to the lack of clarity regarding the number of cycles required to achieve the measured surface hardness.

4.3. Influence of wear transition

Figure 3 illustrates that, with the exception of Mn13 at 1 800 MPa, the wear rates of the driving wheel discs are higher than those of the driven rail discs. Hu et. al. [39] compared the wear rates of driving and driven discs and found that driving discs exhibits higher wear rates, which is consistent with the results presented in Figure 3. This indicates, as previously stated, that mild wear is dominant. However, this does not apply to Mn13 at 1 800 MPa. Due to the significant increase in the wear rate of Mn13 from 1 400 MPa to 1 800 MPa, a transition from mild to severe wear may have occurred. Accordingly, the prevailing tenet that comparable $T\gamma/A$ values should result in comparable wear rates and wear regimes [37], does not appear to be applicable to Mn13.

5. Conclusion

Twin disc tests have been performed for advanced rail materials used in crossing applications. The test results indicate that the fine-pearlitic R400HT has the highest wear resistance compared to the other materials tested. The wear rates of bainitic CrB1400 are slightly higher than those of R400HT. This suggests that R400HT and CrB1400 demonstrate superior wear resistance under the specified test conditions. The wear behavior of the austenitic Mn13 differs quite significantly from that of the high-strength steels due to its low initial hardness and a distinctive wear mechanism. At a contact pressure of 1 800 MPa, Mn13 may have been subjected to severe wear, whereas the other tests were conducted in the mild wear regime. It is obvious that differences exist between twin disc tests and real crossing applications, see [20]. The authors assume that EDH has a positive influence on the wear resistance of Mn13. Consequently, it is recommended that Mn13 crossings are pre-hardened by EDH, given the high contact pressures that are likely to occur in such crossings. However, since uncertainties remain about the wear mechanism in the austenitic Mn13, further research, such as the analysis of the running surface, is suggested.

6. Acknowledgements

The authors gratefully acknowledge the financial support under the scope of the COMET program within the K2 Center “Integrated Computational Material, Process and Product Engineering (IC-MPPE)” (Project No 886385). This program is supported by the Austrian Federal Ministries for Climate Action, Environment, Energy, Mobility, Innovation and Technology (BMK) and for Labour and Economy (BMAW), represented by the Austrian Research Promotion Agency (FFG), and the federal states of Styria, Upper Austria and Tyrol.

References

- [1] I. Grossoni, P. Hughes, Y. Bezin, A. Bevan, J. Jaiswal, Observed failures at railway turnouts: Failure analysis, possible causes and links to current and future research, *Engineering Failure Analysis* 119 (2021) 104987.
- [2] M. Pletz, W. Daves, W. Yao, H. Ossberger, Rolling contact fatigue of three crossing nose materials—multiscale fe approach, *Wear* 314 (2014) 69–77.
- [3] J. Wiedorn, W. Daves, U. Ossberger, H. Ossberger, M. Pletz, Simplified explicit finite element model for the impact of a wheel on a crossing – validation and parameter study, *Tribology International* 111 (2017) 254–264.
- [4] A. Johansson, B. Pålsson, M. Ekh, J. C. Nielsen, M. K. Ander, J. Brouzoulis, E. Kassa, Simulation of wheel–rail contact and damage in switches & crossings, *Wear* 271 (2011) 472–481.
- [5] S. Eck, H. Oßberger, U. Oßberger, S. Marsoner, R. Ebner, Comparison of the fatigue and impact fracture behaviour of five different steel grades used in the frog of a turnout, *Proceedings of the Institution of Mechanical Engineers, Part F: Journal of Rail and Rapid Transit* 228 (2014) 603–610.
- [6] M. Schilke, J. Ahlström, B. Karlsson, Low cycle fatigue and deformation behaviour of austenitic manganese steel in rolled and in as-cast conditions, *Procedia Engineering* 2 (2010) 623–628.
- [7] voestalpine Railway Systems, 400 uhc hsh product line, 2023. URL: <https://www.voestalpine.com/railway-systems/de/produkte/400-uhc-hsh-schiene/>.
- [8] M. Faccoli, A. Ghidini, A. Mazzù, Changes in the microstructure and mechanical properties of railway wheel steels as a result of the thermal load caused by shoe braking, *Metallurgical and Materials Transactions A* 50 (2019) 1701–1714.
- [9] J. Wiedorn, W. Daves, U. Ossberger, H. Ossberger, M. Pletz, Finite element model for predicting the initiation of subsurface damage in railway crossings—a parametric study, *Proceedings of the Institution of Mechanical Engineers, Part F: Journal of Rail and Rapid Transit* 233 (2019) 614–628.
- [10] M. Lukas, G. Ressel, C. Hahn, S. Eck, B. Sartory, T. Titze, U. Ossberger, Detwinning phenomenon and its effect on resulting twinning structure of an austenitic hadfield steel, *Metallurgical and Materials Transactions A* 54 (2023) 1286–1295.
- [11] F. C. Zhang, B. Lv, T. S. Wang, C. L. Zheng, M. Zhang, H. H. Luo, H. Liu, A. Y. Xu, Explosion hardening of hadfield steel crossing, *Materials Science and Technology* 26 (2010) 223–229.
- [12] R. Lewis, E. Magel, W.-j. Wang, U. Olofsson, S. Lewis, T. Slatter, A. Beagles, Towards a standard approach for the wear testing of wheel and rail materials, *Proceedings of the Institution of Mechanical Engineers, Part F: Journal of Rail and Rapid Transit* 231 (2017) 760–774.
- [13] J. F. Santa, P. Cuervo, P. Christoforou, M. Harmon, A. Beagles, A. Toro, R. Lewis, Twin disc assessment of wear regime transitions and rolling contact fatigue in r400ht – e8 pairs, *Wear* 432–433 (2019) 102916.
- [14] Y. Hu, L. C. Guo, M. Maiorino, J. P. Liu, H. H. Ding, R. Lewis, E. Meli, A. Rindi, Q. Y. Liu, W. J. Wang, Comparison of wear and

- rolling contact fatigue behaviours of bainitic and pearlitic rails under various rolling-sliding conditions, *Wear* 460-461 (2020) 203455.
- [15] F. Braghin, R. Lewis, R. S. Dwyer-Joyce, S. Bruni, A mathematical model to predict railway wheel profile evolution due to wear, *Wear* 261 (2006) 1253–1264.
- [16] J. Liu, W. Jiang, S. Chen, Q. Liu, Effects of rail materials and axle loads on the wear behavior of wheel/rail steels, *Advances in Mechanical Engineering* 8 (2016) 168781401665725.
- [17] R. Lewis, U. Olofsson, Mapping rail wear regimes and transitions, *Wear* 257 (2004) 721–729.
- [18] C. Kammerhofer, A. Hohenwarter, R. Pippan, A novel laboratory test rig for probing the sensitivity of rail steels to rcf and wear – first experimental results, *Wear* 316 (2014) 101–108.
- [19] J. W. Ringsberg, A. Skyttebol, B. L. Josefson, Investigation of the rolling contact fatigue resistance of laser clad twin-disc specimens: Fe simulation of laser cladding, grinding and a twin-disc test, *International Journal of Fatigue* 27 (2005) 702–714.
- [20] M. Kráčalík, W. Daves, T. Antretter, Calculation of crack driving forces of surface cracks subjected to rolling/sliding contact, *Engineering Fracture Mechanics* 152 (2016) 10–25.
- [21] H. Al-Maliki, A. Meierhofer, G. Trummer, R. Lewis, K. Six, A new approach for modelling mild and severe wear in wheel-rail contacts, *Wear* 476 (2021) 203761.
- [22] P. Christoforou, D. I. Fletcher, R. Lewis, Benchmarking of premium rail material wear, *Wear* 436-437 (2019) 202990.
- [23] R. Lewis, P. Christoforou, W. J. Wang, A. Beagles, M. Burstow, S. R. Lewis, Investigation of the influence of rail hardness on the wear of rail and wheel materials under dry conditions (icri wear mapping project), *Wear* 430-431 (2019) 383–392.
- [24] M. Harmon, J. F. Santa, J. A. Jaramillo, A. Toro, A. Beagles, R. Lewis, Evaluation of the coefficient of friction of rail in the field and laboratory using several devices, *Tribology - Materials, Surfaces & Interfaces* 14 (2020) 119–129.
- [25] R. Lewis, R. S. Dwyer-Joyce, Wear mechanisms and transitions in railway wheel steels, *Proceedings of the Institution of Mechanical Engineers, Part J: Journal of Engineering Tribology* 218 (2004) 467–478.
- [26] Y. Hu, M. Watson, M. Maiorino, L. Zhou, W. J. Wang, H. H. Ding, R. Lewis, E. Meli, A. Rindi, Q. Y. Liu, J. Guo, Experimental study on wear properties of wheel and rail materials with different hardness values, *Wear* 477 (2021) 203831.
- [27] M. Messaadi, M. Oomen, A. Kumar, Friction modifiers effects on tribological behaviour of bainitic rail steels, *Tribology International* 140 (2019) 105857.
- [28] Q. Luo, M. Kitchen, J. Li, W. Li, Y. Li, Experimental investigation on the spalling failure of a railway turnout made from hadfield steel, *Wear* 523 (2023) 204779.
- [29] Q. Luo, J. Zhu, Wear property and wear mechanisms of high-manganese austenitic hadfield steel in dry reciprocal sliding, *Lubricants* 10 (2022) 37.
- [30] V. H. Mercado, I. Mejía, A. Bedolla-Jacuinde, Effect of load and sliding rate on the wear behavior of ti-containing twip steel, *Journal of Materials Engineering and Performance* 26 (2017) 2213–2225.
- [31] M. Lindroos, M. Apostol, V. Heino, K. Valtonen, A. Laukkanen, K. Holmberg, V.-T. Kuokkala, The deformation, strain hardening, and wear behavior of chromium-alloyed hadfield steel in abrasive and impact conditions, *Tribology Letters* 57 (2015).
- [32] X. Qiu, X. Wei, X. Xu, W. Xu, M. Zhu, Dependence of fretting wear resistance on microstructural features of alloyed steels, *Tribology International* 137 (2019) 39–45.
- [33] P. J. Bolton, P. Clayton, Rolling—sliding wear damage in rail and tyre steels, *Wear* 93 (1984) 145–165.
- [34] W. J. Wang, R. Lewis, B. Yang, L. C. Guo, Q. Y. Liu, M. H. Zhu, Wear and damage transitions of wheel and rail materials under various contact conditions, *Wear* 362-363 (2016) 146–152.
- [35] H. Soleimani, M. Moavenian, Tribological aspects of wheel–rail contact: A review of wear mechanisms and effective factors on rolling contact fatigue, *Urban Rail Transit* 3 (2017) 227–237.
- [36] D. I. Fletcher, J. H. Beynon, Development of a machine for closely controlled rolling contact fatigue and wear testing, *Journal of Testing and Evaluation* 28 (2000) 267.
- [37] C. Hardwick, R. Lewis, D. T. Eadie, Wheel and rail wear—understanding the effects of water and grease, *Wear* 314 (2014) 198–204.
- [38] Y. Hu, L. Zhou, H. H. Ding, G. X. Tan, R. Lewis, Q. Y. Liu, J. Guo, W. J. Wang, Investigation on wear and rolling contact fatigue of wheel-rail materials under various wheel/rail hardness ratio and creepage conditions, *Tribology International* 143 (2020) 106091.
- [39] Y. Hu, W. J. Wang, M. Watson, K. Six, H. Al-Maliki, A. Meierhofer, R. Lewis, Wear of driving versus driven discs in a twin disc rolling-sliding test, *Wear* 512-513 (2023) 204528.
- [40] B. White, Z. S. Lee, R. Lewis, Towards a standard approach for the twin disc testing of top-of rail friction management products, *Lubricants* 10 (2022) 124.
- [41] R. Lewis (Ed.), *Wheel-rail interface handbook*, Woodhead publishing in mechanical engineering, CRC Press and Woodhead, Boca Raton, Fla. and Oxford u. a., 2009.
- [42] R. Skrypnik, M. Ekh, J. C. Nielsen, B. A. Pålsson, Prediction of plastic deformation and wear in railway crossings – comparing the performance of two rail steel grades, *Wear* 428-429 (2019) 302–314.
- [43] R. Skrypnik, U. Ossberger, B. A. Pålsson, M. Ekh, J. C. Nielsen, Long-term rail profile damage in a railway crossing: Field measurements and numerical simulations, *Wear* 472-473 (2021) 203331.
- [44] L. Qian, M. Li, Z. Zhou, H. Yang, X. Shi, Comparison of nano-indentation hardness to microhardness, *Surface and Coatings Technology* 195 (2005) 264–271.